TECHNISCHE UNIVERSITÄT
KAISERSLAUTERN

SCHRIFTEN ZUR

FUNKTIONALANALYSIS UND GEOMATHEMATIK

V. Michel, K. Wolf

Numerical Aspects of a Spline-Based Multiresolution Recovery of the Harmonic Mass Density out of Gravity Functionals

Bericht 28 – November 2006

FACHBEREICH MATHEMATIK

Numerical Aspects of a Spline-Based Multiresolution Recovery of the Harmonic Mass Density out of Gravity Functionals

Volker Michel, Kerstin Wolf
Geomathematics Group
Department of Mathematics
University of Kaiserslautern
P.O. Box 3049
67653 Kaiserslautern
Germany
Email: michel@mathematik.uni-kl.de, kerstin-wlf@gmx.de
WWW: http://www.mathematik.uni-kl.de/∼wwwgeo

November 23, 2006

Abstract We show the numerical applicability of a multiresolution method based on harmonic splines on the 3-dimensional ball which allows the regularized recovery of the harmonic part of the Earth's mass density distribution out of different types of gravity data, e.g. different radial derivatives of the potential, at various positions which need not be located on a common sphere. This approximated harmonic density can be combined with its orthogonal anharmonic complement, e.g. determined out of the splitting function of free oscillations, to an approximation of the whole mass density function. The applicability of the presented tool is demonstrated by several test calculations based on simulated gravity values derived from EGM96. The method yields a multiresolution in the sense that the localization of the constructed spline basis functions can be increased which yields in combination with more data a higher resolution of the resulting spline. Moreover, we show that a locally improved data situation allows a highly resolved recovery in this particular area in combination with a coarse approximation elsewhere which is an essential advantage of this method, e.g. compared to polynomial approximation.

Keywords multiresolution, spline, inverse problem, numerical implementation, gravimetry, CHAMP, GRACE, GOCE, SST, SGG, EGM96, satellite data, localization, harmonic density.

AMS(2000) Classification: 45B05, 45Q05, 65D07, 65R30, 86A22

1 Introduction

Already for a long time, people are interested in the interior of the Earth. So, a classical problem in geophysics and physical geodesy is the determination of the Earth's mass density distribution. In general, the determination of the structures in the Earth's interior is usually realized by analyzing two types of data, namely either the gravitational data or the seismic data. This paper studies the gravimetry problem, i.e. we reconstruct the density variations inside and on the Earth's surface from the gravitational potential and its functionals on and outside the Earth. This problem and related ones have been discussed by several authors before, see e.g. [1, 2, 3, 4, 5, 6, 9, 12, 13, 15, 16, 17, 19, 20, 21, 22, 23, 24, 25, 26, 27, 28, 29, 30, 31, 32] and the references therin.

From the mathematical point of view, the gravimetry problem is based on a Fredholm integral equation of the first kind involving Newton's law of gravitation. Thus, the relation between the gravitational potential V of the Earth and the density distribution ρ is given by

$$V(y) = \int\limits_{\text{Earth}} \frac{\rho(x)}{|x-y|}\, dx.$$

In reality, the gravitational potential V can be determined for the Earth whereas the density ρ represents the unknown part. This means that we have to consider the inversion of the equation above. Problems of such kind are called inverse problems.
By Hadamard's classification, that is the uniqueness, the existence and the stability of the solution, we divide inverse problems in ill-posed and well-posed problems. It is a well-known fact that the gravimetry problem is ill-posed because each of these three criteria can be invalid.

For finding an approximation for the solution of such an ill-posed inverse problem several different methods are developed. The classical approach, for example, is a method using a truncated singular value decomposition. This method has several well-known disadvantages like the non-localizing character of the used spherical harmonics and the bandlimitedness of the solution. Modern methods apply regularization techniques which use wavelets. With such a method we can locally reconstruct our solution by applying kernels that are only essentially large in the interesting region.

In this paper we briefly explain the already existing theory of a regularization method for the gravimetry problem from measurements of satellite data using a spline-based multiresolution (see, thereto, [10]). Afterwards, in more details we present the corresponding numerical realization. Such an approach has several advantages. On the one hand, it includes the well-known useful spline properties like the smoothing and the best approximating properties. And, on the other hand, we can arbitrarily distribute the satellite data in the outer space of the Earth. For comparison, the wavelet methods developed for example in [20, 21, 22, 23, 24] demand the data to be located on a spherical domain. This advantage of the spline approach includes, in particular, the possibility to mix data from different satellite missions. So, we can combine different orbits and different derivatives of the gravitational potential in the calculations of the Earth's density distribution. For testing this method we use, for the gravitational potential, its first radial derivative and its second radial derivative, a model generated out of EGM96, i.e. the "Earth Gravity Model 96" (see [18]), where the potential is represented by spherical harmonics. Modern satellite techniques like SST (satellite-to-satellite tracking) used in the case of the satellites CHAMP (Challenging Minisatellite Payload, launch: 7/15/2000) and GRACE (Gravity Recovery and Climate Experiment, launch: 3/17/2002) and SGG (satellite gravity gradiometry) intended for the planned mission GOCE (Gravity and Steady-State Ocean Circulation Explorer, launch: 2007) yield data from which we can derive the derivatives of the gravitational potential. For the presented method, a combination with these modern satellite techniques can also be calculated in the future. More precisely, the gradient of V, in particular the first radial derivative, is a part of SST generated on a point grid in about 400 km altitude whereas the Hessian of V, in particular the second radial derivative, is a part of SGG generated on a point grid in about 200 km altitude. In this framework

we use an equiangular point grid and we simplify the Earth and the orbits as a ball and spheres, respectively, where the latter is not a requirement of the method.
Furthermore, by the multiresolution spline approach, the approximating splines can be calculated at different scales, such that we get for a higher scale a better resolution for the reconstruction of the Earth's interior, that is by decreasing the hat-width and, at the same time, by adding at each step more and more data.

In this paper we first explain briefly the principles of the spline method for the approximation of the harmonic density distribution and, then, the new numerical results are discussed.

2 Preliminaries

2.1 Spherical Functions

In order to translate the explained gravimetry problem into a spline interpolation problem we need the following mathematical background:
Each point of the three-dimensional Euclidean space $\mathbb{R}^3$, $x = (x_1, x_2, x_3)^{\mathrm{T}}$, $|x| \neq 0$, allows a unique representation of the form $x = r\xi$, $r = |x|$, $\xi = (\xi_1, \xi_2, \xi_3)^{\mathrm{T}}$, where $\xi \in \mathbb{R}^3$, $|\xi| = 1$, is the uniquely determined directional unit vector of $x \in \mathbb{R}^3 \setminus \{0\}$. The unit sphere in $\mathbb{R}^3$ is denoted by Ω, i.e. $\Omega = \{\xi \in \mathbb{R}^3 \mid |\xi| = 1\}$. For the gravimetry problem we assume that the Earth has the shape of a ball with radius $\beta = 6\,378\,136.3\,\mathrm{m}$. So, the surface, i.e. the sphere with center 0 and radius β, is denoted by B. B_{int} and $B_{\mathrm{ext}} = \mathbb{R}^3 \setminus \overline{B_{\mathrm{int}}}$ describe the Earth's interior and exterior, respectively.
As usual, we introduce the spherical harmonics as restrictions of homogeneous harmonic polynomials to Ω. More precisely, let $H_n : \mathbb{R}^3 \to \mathbb{R}$ be a homogeneous harmonic polynomial of degree $n \in \mathbb{N}_0$, then the restriction $Y_n = H_n|_\Omega$ is called a spherical harmonic of degree n. The space of all spherical harmonics of degree n is denoted by $\mathrm{Harm_n}(\Omega)$, and its dimension is known to be $\dim(\mathrm{Harm_n}(\Omega)) = 2\mathrm{n} + 1$. Spherical harmonics of different degrees are orthogonal in the sense of the $\mathrm{L}^2(\Omega)$-inner product, i.e.

$$(Y_n, Y_m)_{\mathrm{L}^2(\Omega)} = \int_\Omega Y_n(\xi) Y_m(\xi)\, d\omega(\xi) = 0,\ n \neq m,$$

where $d\omega$ is the surface element on Ω. Moreover, the set of spherical harmonics $Y_{n,j}$ of degree $n \in \mathbb{N}_0$ and order $j = 1, \ldots, 2n+1$ forms an orthonormal basis of $\mathrm{L}^2(\Omega)$. Any spherical harmonic Y_n, $n \in \mathbb{N}_0$, is an infinitely often differentiable eigenfunction of the Beltrami operator Δ^* corresponding to the eigenvalue $(\Delta^*)^\wedge(n) = -n(n+1)$, i.e. $\Delta^*_\xi Y_n(\xi) = -n(n+1)Y_n(\xi)$, $\xi \in \Omega$, $Y_n \in \mathrm{Harm_n}(\Omega)$. The well-known addition theorem shows the relation between the spherical harmonics $\{Y_{n,j}\}_{j=1,\ldots,2n+1}$ and the also well-known Legendre polynomials P_n of degree $n \in \mathbb{N}_0$:

$$\sum_{k=1}^{2n+1} Y_{n,k}(\xi) Y_{n,k}(\eta) = \frac{2n+1}{4\pi} P_n(\xi \cdot \eta) \quad ;\ \xi, \eta \in \Omega.$$

2.2 Inner Harmonics

Because, in this paper, we are interested in the harmonic part of the Earth's density distribution we consider the harmonic functions on the ball B_{int}. The set of all these functions is denoted by $\mathrm{Harm}(\mathrm{B_{int}}) = \left\{\mathrm{F} \in \mathrm{C}^2(\mathrm{B_{int}}) \mid \Delta \mathrm{F} = 0 \text{ in } \mathrm{B_{int}}\right\}$, where $\Delta F = (\frac{\partial^2}{\partial x_1^2} + \frac{\partial^2}{\partial x_2^2} + \frac{\partial^2}{\partial x_3^2})F(x)$ is the Laplace operator. Further, for all $n \in \mathbb{N}_0$, $j = 1, \ldots, 2n+1$, the inner harmonics are defined by

$$H^B_{n,j}(x) = \sqrt{\frac{2n+3}{\beta^3}} \left(\frac{|x|}{\beta}\right)^n Y_{n,j}\left(\frac{x}{|x|}\right),\ x \in B_{\mathrm{int}}.$$

Indeed the inner harmonics are not dense in $\mathrm{L}^2(B_{\mathrm{int}})$ as the spherical harmonics in $\mathrm{L}^2(\Omega)$, but nevertheless they constitute a linear strict subspace of $\mathrm{L}^2(B_{\mathrm{int}})$. Moreover, the orthonormal system $\left\{H^B_{n,j}\right\}_{n\in\mathbb{N}_0,\ j=1,\ldots,2n+1}$ is complete in the Hilbert space $\left(\mathrm{Harm}(\mathrm{B_{int}}), (\cdot,\cdot)_{\mathrm{L}^2(\mathrm{B_{int}})}\right)$.

2.3 Formulation of the Gravimetry Problem

Gravimetry means the determination of the Earth's mass density distribution from measurements of the gravitational potential. It is a classical problem in geophysics and physical geodesy and an important application of the (geo)potential theory. Such a problem ranks among inverse problems. The inverse problem is the task that is often found in science and mathematics where the values of model parameters must be obtained via observed data.
From the mathematical point of view, the relation between the gravitational potential of the Earth and the density distribution is given by the Fredholm integral equation of first kind involving Newton's law of gravitation (see, e.g. [14, 22, 33]):

$$(T\rho)(y) = \int\limits_{B_{\text{int}}} \frac{\rho(x)}{|x-y|}\, dx = V(y),\ y \in B_{\text{ext}}.$$

Here, $\rho \in \mathrm{L}^2(B_{\text{int}})$ represents the unknown mass density function and V the gravitational potential which is in practice only given on a finite point set. The inversion of this equation, then, is called gravimetry problem.
It is a well-known fact that the space $\mathrm{L}^2(B_{\text{int}})$ needed for this problem can be decomposed in a direct sum of the closed linear subspace $\mathrm{Harm}(\mathrm{B}_{\text{int}})$ and its $\mathrm{L}^2(B_{\text{int}})$-orthogonal space $\mathrm{Anharm}(B_{\text{int}})$. Since this anharmonic space constitutes the null space of the operator T, only the harmonic part of the density distribution can be explored from the gravitational potential. For this reason, we restrict here our attention to the recovery of the harmonic part. The anharmonic part should be determined from, e.g., seismic data and added to the result by the described method. This anharmonic modelling (see also [2, 3, 4, 5, 11, 21, 22]) is a challenge for future research.
Furthermore, this inverse problem fulfills not even one of the three Hadamard's criteria (existence, uniqueness and stability) for a well-posed problem. It turns out that the gravimetry problem is even an exponentially ill-posed problem which can be regularized by the method described here, i.e. the solution can be approximated in a stable way.

3 Multiresolution Analysis of Harmonic Splines

Since the density can only be determined via an inverse problem with discretely given data we represent the given information by linear continuous functionals $\mathcal{F}_1, ..., \mathcal{F}_N$. Examples of such functionals are 0th to 2nd order radial derivatives of the corresponding gravitational potential at certain points $x_k \in B_{\text{ext}}$ outside the Earth. We define

$$\begin{aligned}
\mathcal{G}_k^{(0)} F &:= \int_{B_{\text{int}}} \frac{F(y)}{|y-x_k|}\, \mathrm{d}y, \\
\mathcal{G}_k^{(1)} F &:= -\left(\frac{x}{|x|} \cdot \nabla_x \int_{B_{\text{int}}} \frac{F(y)}{|y-x|}\, \mathrm{d}y \right)\Big|_{x=x_k}, \\
\mathcal{G}_k^{(2)} F &:= \left(\frac{x}{|x|} \cdot \left(\left(\nabla_x \otimes \nabla_x \int_{B_{\text{int}}} \frac{F(y)}{|y-x|}\, \mathrm{d}y \right) \frac{x}{|x|} \right) \right)\Big|_{x=x_k}.
\end{aligned}$$

We assume the density F to be in a certain subspace $\mathcal{H}_J := \mathcal{H}(\{\varphi_J(n)\}; B_{\text{int}}) \subset \mathrm{Harm}\,(B_{\text{int}})$, $J \in \mathbb{N}_0$ fixed, which is determined by a real sequence $\{\varphi_J(n)\}_{n\in\mathbb{N}_0}$ and contains all functions $F \in \mathrm{Harm}\,(B_{\text{int}})$ such that

$$\left(F, H_{n,j}^B\right)_{\mathrm{L}^2(B_{\text{int}})} = 0 \text{ for all } n \in \mathbb{N}_0 \text{ with } \varphi_J(n) = 0$$

and

$$\|F\|_{\mathcal{H}_J}^2 := \sum_{\substack{n=0 \\ \varphi_J(n)\neq 0}}^{\infty} \sum_{j=1}^{2n+1} \left(\varphi_J(n)\right)^{-2} \left(F, H_{n,j}^B\right)_{\mathrm{L}^2(B_{\text{int}})}^2 < +\infty. \tag{1}$$

Usually, $\varphi_J(n) \to 0$ as $n \to \infty$ will hold. Hence, $(\varphi_J(n))^{-2} \to +\infty$ as $n \to \infty$. Thus, the norm $\|F\|_{\mathcal{H}_J}$ will significantly increase if F has a high energy at large inner harmonics degrees. In this

sense, this norm is a measure for the non–smoothness of F. Moreover, the faster $\varphi_J(n)$ tends to 0 as $n \to \infty$, i.e. the more rapidly $(\varphi_J(n))^{-2}$ diverges, the stronger is condition (1). Indeed, one can prove the following result.

Theorem 3.1
If the sequences $\{\varphi_J(n)\}_{n\in\mathbb{N}_0}$, $J \in \mathbb{N}_0$, satisfy

(i) $0 \le \varphi_J(n) \le \varphi_{J+1}(n) \le 1$ *for all* $n, J \in \mathbb{N}_0$ *(monotonicity),*

(ii) $\sum_{n=0}^{\infty}(\varphi_J(n))^2 n^2 < +\infty$ *for all* $J \in \mathbb{N}_0$ *(summability),*

(iii) For every fixed $n \in \mathbb{N}_0$ *the sequence* $\{\varphi_J(n)\}_{J\in\mathbb{N}_0}$ *is not identical to* 0*, i.e. there exists* j_n *such that* $\varphi_J(n) > 0$ *for all* $J \ge j_n$ *(non–triviality),*

then the spaces $\mathcal{H}_J = \mathcal{H}(\{\varphi_J(n)\}; B_{\rm int})$ *define a multiresolution analysis, i.e.*

a) $\mathcal{H}_J \subset \mathcal{H}_{J+1} \subset \mathcal{H}(\{\varphi(n)\}; B_{\rm int}) \subset \mathrm{Harm}\,(B_{\rm int})$ *for all* $J \in \mathbb{N}_0$,

b) $\overline{\bigcup_{J\in\mathbb{N}_0}\mathcal{H}_J}^{\|.\|_{\mathcal{H}(\{\varphi(n)\};B_{\rm int})}} = \mathcal{H}(\{\varphi(n)\}; B_{\rm int}) =: \mathcal{H}_\infty$,

where $\varphi(n) := \lim_{J\to\infty}\varphi_J(n)$ *for each* $n \in \mathbb{N}_0$. *Moreover, if* $\varphi(n) = 1$ *for all* $n \in \mathbb{N}_0$ *then* $\mathcal{H}_\infty = \mathrm{Harm}\,(B_{\rm int})$.

This means that we get a nested sequence of spaces. The larger J is, the "more" functions are available and the higher the resolution can be expected to be. Furthermore, every function in $\mathrm{Harm}\,(B_{\rm int})$ can be approximated arbitrarily well by an element of $\mathcal{H}_J$ if J is large enough, provided that the sequences were chosen appropriately.
To construct splines we have to realize that the summability condition (see Theorem 3.1) implies the existence and uniqueness of a so–called reproducing kernel which can here be represented by

$$\begin{aligned} K_{\mathcal{H}_J}(x,y) &= \sum_{n=0}^{\infty}\sum_{j=1}^{2n+1}(\varphi_J(n))^2\, H^B_{n,j}(x)H^B_{n,j}(y) \\ &= \sum_{n=0}^{\infty}(\varphi_J(n))^2\,\frac{(2n+3)(2n+1)}{4\pi\beta^3}\,P_n\left(\frac{x}{|x|}\cdot\frac{y}{|y|}\right)\left(\frac{|x|\,|y|}{\beta^2}\right)^n, \end{aligned}$$

$x, y \in B_{\rm int}$, where P_n is the Legendre polynomial of degree n. Provided that our data may be represented as evaluation of a linearly independent set of linear and continuous functionals $\{\mathcal{F}_1, ..., \mathcal{F}_N\} =: \mathcal{F}$, which could, for instance, have the form of the derivatives $\mathcal{G}_k^{(l)}$ defined above, then any function $S \in \mathcal{H}_J$ of the form

$$S(y) = \sum_{j=1}^{N} a_j \mathcal{F}_j K_{\mathcal{H}_J}(\cdot, y), \quad y \in B_{\rm int},$$

with coefficients $a_1, ..., a_N \in \mathbb{R}$ is called harmonic spline at scale J relative to $\mathcal{F}$. Here, $\mathcal{F}_j K_{\mathcal{H}_J}(\cdot, y)$ means that y is kept fixed and $K_{\mathcal{H}_J}(\cdot, y)$ is merely considered as a function of the first argument to which $\mathcal{F}_j$ is applied.

Theorem 3.2
If $\mathcal{F} = \{\mathcal{F}_1, ..., \mathcal{F}_N\}$ *is a linearly independent system of linear and continuous real functionals on* $\mathcal{H}_J$ *and* $y \in \mathbb{R}^N$ *is a given vector then there exists one and only one spline* $S(y) = \sum_{j=1}^{N} a_j \mathcal{F}_j K_{\mathcal{H}_J}(\cdot, y)$, $y \in B_{\rm int}$, *such that*

$$\mathcal{F}_k S = y_k \text{ for all } k = 1, ..., N. \tag{2}$$

The coefficients $a_1, ..., a_N$ *of this spline are given by the positive definite system of linear equations*

$$\sum_{j=1}^{N} a_j \mathcal{F}_k \mathcal{F}_j K_{\mathcal{H}_J}(\cdot,\cdot) = y_k \text{ for all } k = 1, ..., N.$$

This means that corresponding to our given information $\mathcal{F}_k S = y_k$ for all $k = 1, ..., N$, e.g. of different radial derivatives of the potential at different positions, there is a unique spline that represents an approximation to the harmonic part of the density in the sense that it reflects the known information. Note that adding a positive diagonal matrix to the matrix of the system above changes the interpolation problem to an approximation problem with a smoother resulting spline. For the calculation of the splines we have to know that

$$\begin{aligned}
\mathcal{F}_i K_{\mathcal{H}_J}(\cdot, y) &= \sum_{n=0}^{\infty} \sum_{j=1}^{2n+1} \left(\varphi_J(n)\right)^2 \left(\mathcal{F}_i H_{n,j}^B\right) H_{n,j}^B(y), \\
\mathcal{F}_k \mathcal{F}_i K_{\mathcal{H}_J}(\cdot, y) &= \sum_{n=0}^{\infty} \sum_{j=1}^{2n+1} \left(\varphi_J(n)\right)^2 \left(\mathcal{F}_i H_{n,j}^B\right) \left(\mathcal{F}_k H_{n,j}^B\right). \qquad (3)
\end{aligned}$$

In case of the above mentioned examples of radial derivatives, i.e. if $\mathcal{F}_k$ is $\mathcal{G}_k^{(l)}$ for $l \in \{0, 1, 2\}$, we have

$$\begin{aligned}
\mathcal{G}_k^{(0)} H_{n,j}^B &= \frac{4\pi}{2n+1} \sqrt{\frac{\beta^3}{2n+3}} \left(\frac{\beta}{|x_k|}\right)^n \frac{1}{|x_k|} Y_{n,j}\left(\frac{x_k}{|x_k|}\right), \\
\mathcal{G}_k^{(1)} H_{n,j}^B &= \frac{n+1}{|x_k|} \frac{4\pi}{2n+1} \sqrt{\frac{\beta^3}{2n+3}} \left(\frac{\beta}{|x_k|}\right)^n \frac{1}{|x_k|} Y_{n,j}\left(\frac{x_k}{|x_k|}\right), \\
\mathcal{G}_k^{(2)} H_{n,j}^B &= \frac{(n+1)(n+2)}{|x_k|^2} \frac{4\pi}{2n+1} \sqrt{\frac{\beta^3}{2n+3}} \left(\frac{\beta}{|x_k|}\right)^n \frac{1}{|x_k|} Y_{n,j}\left(\frac{x_k}{|x_k|}\right).
\end{aligned}$$

Hence, the matrix of the system of linear equations may be represented by

$$\begin{aligned}
\mathcal{G}_i^{(l)} \mathcal{G}_k^{(m)} K_{\mathcal{H}_J}(\cdot, \cdot) &= \sum_{n=0}^{\infty} \sum_{j=1}^{2n+1} \left(\varphi_J(n)\right)^2 \left(\mathcal{G}_i^{(l)} H_{n,j}^B\right) \left(\mathcal{G}_k^{(m)} H_{n,j}^B\right) \\
&= \sum_{n=0}^{\infty} \left(\varphi_J(n)\right)^2 \frac{4\pi}{2n+1} \frac{\beta^3}{2n+3} \left(\frac{\beta^2}{|x_i|\,|x_k|}\right)^n P_n\left(\frac{x_i}{|x_i|} \cdot \frac{x_k}{|x_k|}\right) \cdot \begin{cases}
\frac{1}{|x_i|\,|x_k|}; & l=0, m=0, \\
\frac{n+1}{|x_i|\,|x_k|^2}; & l=0, m=1, \\
\frac{n+1}{|x_i|^2|x_k|}; & l=1, m=0, \\
\frac{(n+1)^2}{|x_i|^2|x_k|^2}; & l=1, m=1, \\
\frac{(n+1)(n+2)}{|x_i|\,|x_k|^3}; & l=0, m=2, \\
\frac{(n+1)(n+2)}{|x_i|^3|x_k|}; & l=2, m=0, \\
\frac{(n+1)^2(n+2)}{|x_i|^2|x_k|^3}; & l=1, m=2, \\
\frac{(n+1)^2(n+2)}{|x_i|^3|x_k|^2}; & l=2, m=1, \\
\frac{(n+1)^2(n+2)^2}{|x_i|^3|x_k|^3}; & l=2, m=2,
\end{cases} \\
&= \sum_{n=0}^{\infty} \left(\varphi_J(n)\right)^2 \frac{4\pi}{2n+1} \frac{\beta^3}{2n+3} \left(\frac{\beta^2}{|x_i|\,|x_k|}\right)^n P_n\left(\frac{x_i}{|x_i|} \cdot \frac{x_k}{|x_k|}\right) \frac{(n+1)^{\delta_{l,1}+\delta_{m,1}} \left(n^2+3n+2\right)^{\delta_{l,2}+\delta_{m,2}}}{|x_i|^{1+l}|x_k|^{1+m}},
\end{aligned}$$

where

$$\delta_{p,q} := \begin{cases} 1, & \text{if } p = q \\ 0, & \text{if } p \neq q \end{cases}$$

is the Kronecker delta.

The obtained series can be truncated for numerical purposes and calculated fast by the Clenshaw algorithm (see [7, 8]).

Splines are typically interpolating functions with maximal smoothness. In our case, the norm $\|\cdot\|_{\mathcal{H}_J}$ serves as a measure for non–smoothness. Indeed, one can show that among all functions $F \in \mathcal{H}_J$ satisfying (2) the interpolating spline of Theorem 3.2 has minimal norm. Moreover, among all splines the interpolating one is closest to the unknown real function F in the sense that it minimizes $\|F - S\|_{\mathcal{H}_J}$ among all splines S at scale J relative to $\mathcal{F}$. Those two characteristics of splines are usually called the 1st and 2nd minimum property.

Since an increasing scale promises a higher resolution we can hope to have a corresponding convergence result, certainly provided that we have enough information and no hole in it. This can be concretized by having a look at the space $\mathcal{H}_\infty^*$ of all continuous linear functionals from $\mathcal{H}_\infty$ to $\mathbb{R}$. We finally arrive at the following convergence theorem.

Theorem 3.3
Assume that the conditions of Theorem 3.1 are satisfied. Let $F \in \bigcup_{J\in\mathbb{N}_0} \mathcal{H}_J$ be a function (the harmonic part of the unknown density function) and $\mathcal{F} := \{\mathcal{F}_i\}_{i\in\mathbb{N}}$ be a (theoretically infinite) linearly independent and closed[1] *system in $\mathcal{H}_\infty^*$. Construct finite subsystems $\mathcal{F}^{(N_J)} := \{\mathcal{F}_1, ..., \mathcal{F}_{N_J}\} \subset \mathcal{F}$, $J \in \mathbb{N}_0$, with increasing size (i.e. $N_J \leq N_{J+1}$ for all $J \in \mathbb{N}_0$) that cover $\mathcal{F}$ (i.e. $\lim_{J\to\infty} N_J = +\infty$). For each scale J determine the unique spline S_J at scale J relative to $\mathcal{F}^{(N_J)}$ such that*

$$\mathcal{F}_i S_J = \mathcal{F}_i F \text{ for all } i = 1, ..., N_J$$

then

$$\lim_{J\to\infty} \|S_J - F\|_{\mathcal{H}_\infty} = 0.$$

Note that each spline S_J continuously depends on the given data vector $(\mathcal{F}_1 F, \ldots, \mathcal{F}_{N_J} F)$ and shows, therefore, only a small sensitivity to added noise.

4 Numerical Results

4.1 Preliminaries

This section deals with the numerical results of the reconstruction of the harmonic projection of the Earth's density distribution.
For our computations we use as a discrete point set the so-called Driscoll-Healy grid, an equiangular latitude-longitude grid. Further we apply data of the gravitational potential generated out of EGM96, i.e. the "Earth Gravity Model 96", which is a spherical harmonic model of the Earth's gravitational potential complete to degree and order 360. As we already mentioned in the introduction of this paper, there are modern satellite techniques as SST and SGG from which we also get data for the derivatives of the gravitational potential. The first radial derivative is a part of SST (CHAMP, GRACE) which is here for our purposes generated on a point grid in 400 km altitude and the second radial derivative of SGG here generated on a point grid in 200 km altitude. Therefore, for our calculations lateron we use different radii with different data sets. Furthermore, three variable symbols $\{\psi_J(n)\}_{n,J}$ are used for the computations. On the one hand two bandlimited sequences, i.e. the Shannon and the cubic polynomial ones, are applied and on the other hand in case of the non-bandlimited kernels we calculate with the Abel-Poisson kernel. For further details on the implementation and additional numerical results we refer to [34].

Remark 4.1
In order to observe more details in the following plots, we have changed the colorbar in dependance on the corresponding image. For achieving a better contrast, we manually set the limits of the colorbar to restrict it to the interesting interval. But to get also the information about the real limits, we endorse each plot with its minimum value and its maximum value which we note by $v_{\min}$ and, accordingly, by $v_{\max}$, both rounded off the integer value. These limits also give us more information about the spline interpolation for example concerning boundary effects.

4.2 Results for the Whole Earth's Surface

In this section we present our results concerning the whole Earth. Thereto, an evaluation point grid with 90 000 points distributed over the whole Earth's surface is applied for plotting the harmonic density distribution. All results are variations of the harmonic density distribution because we calculate without degrees $0, 1$ and 2 which we eliminate by setting them equal to 0. Fig. 1(a) shows us

[1] This means that every functional in $\mathcal{H}_\infty^*$ can be approximated arbitrarily well by a finite linear combination of functionals in $\mathcal{F}$. In other words, there is no information related to F that cannot be approximately described by the already given data.

the harmonic density distribution which is computed out of the potential at 6 320 given data points given on an equiangular grid with radius $r_0 = \beta \cdot 1.001$. The kernel is generated by the bandlimited Shannon sequence at scale $J = 9$. In this figure we can clearly see, that we have insufficient data points for such a high scale because we can recognize the several data points between all evaluation points. This means that our hat-width is too small, and, therefore, Fig. 1(b) presents the same result where we apply more, i.e. 14 280, data points. Here, we can no longer identify so clearly each data point but nevertheless, it is not a satisfactory result for the gravimetry problem. Since we have also attained the limits of the memory capacity of our computers we, consequently, try another way, namely by changing the sequence for the kernels. For another bandlimited example (see Fig. 2(a)) we use the sequence generated by a cubic polynomial at scale $J = 9$ and in case of the non-bandlimited example (Fig. 2(b)) we utilize the Abel-Poisson sequence at scale $J = 5$.
Comparing all these figures, one can assume that the results applying the cubic polynomial kernel yields better solutions than those calculated by the Shannon kernel and with the Abel-Poisson kernel we achieve a really good approximation of the harmonic density distribution. As reference we can use independent recoveries of the harmonic density out of EGM96 such as in [24].
First of all, we can clearly recognize most of the coastlines. So, we are able to see the continents as North and South America, Africa and Australia. The continents Europe and Asia cannot explicitly be represented by this reconstruction, but nevertheless we can realize the Himalayas in the North of India, the Java Trench near Indonesia, the mid-Atlantic ridge, the mountain range underwater near Japan and the Andes in the West of South America.

In the next section, we consider just a small part of the Earth because we want to determine locally the Earth's interior which is one advantage of the developed method. Localizing also allows us to apply a point grid where the points lie closer to each other than that which we used for the figures in this section.

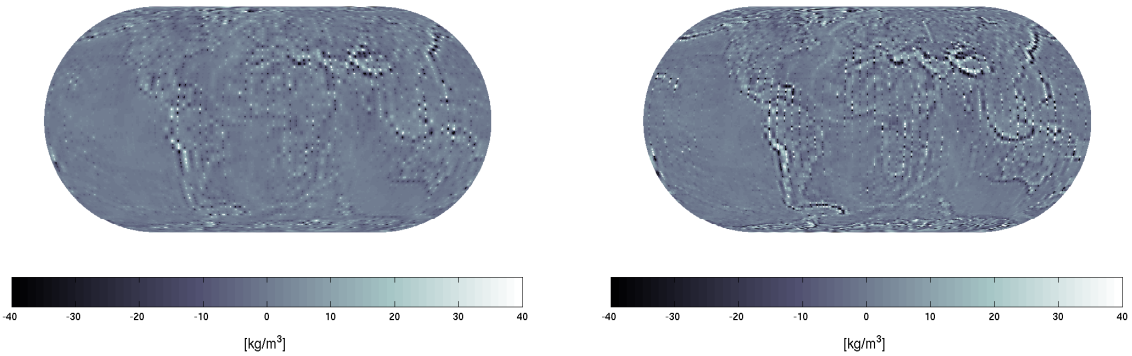

(a) Computed from 6 320 data points at scale $J = 9$, $\left(v_{\min} \approx -200\,\frac{\mathrm{kg}}{\mathrm{m}^3},\ v_{\max} \approx 132\,\frac{\mathrm{kg}}{\mathrm{m}^3}\right)$.

(b) Computed from 14 280 data points at scale $J = 9$, $\left(v_{\min} \approx -239\,\frac{\mathrm{kg}}{\mathrm{m}^3},\ v_{\max} \approx 232\,\frac{\mathrm{kg}}{\mathrm{m}^3}\right)$.

Figure 1: Variation of the harmonic density distribution computed with the Shannon sequence.

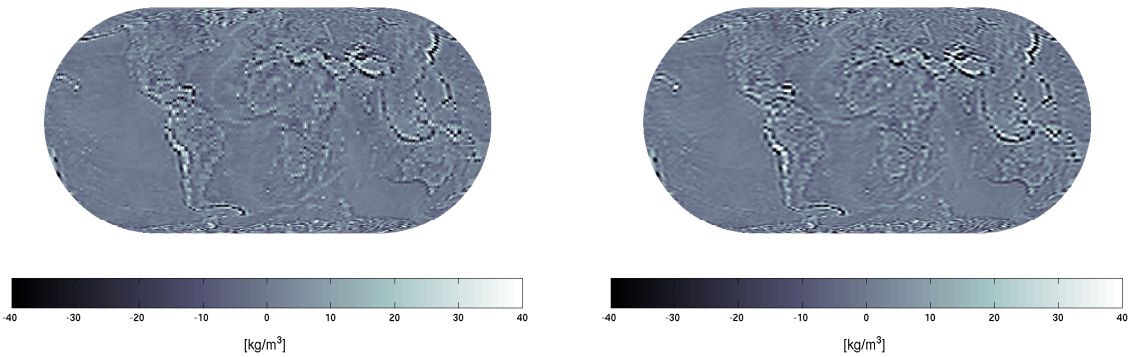

(a) Computed with the kernel generated by a cubic polynomial at scale $J = 9$, $\left(v_{\min} \approx -180\ \frac{\text{kg}}{\text{m}^3},\ v_{\max} \approx 138\ \frac{\text{kg}}{\text{m}^3}\right)$.

(b) Computed with the Abel-Poisson kernel at scale $J = 5$, $\left(v_{\min} \approx -136\ \frac{\text{kg}}{\text{m}^3},\ v_{\max} \approx 115\ \frac{\text{kg}}{\text{m}^3}\right)$.

Figure 2: Variation of the harmonic density distribution computed from 14 280 data points.

4.3 Results for South America

In this section we restrict our exploring domain in order to apply the developed method only to a part of the Earth. We want to show that with this spline interpolation method we can also calculate the harmonic density distribution locally. This means that we make further considerations only for a relatively small part of the Earth, namely for South America. Because of this restriction we are able to explore this region using point grids, where the points are closer to each other than those of a point grid for the whole Earth's surface. Thus, we present here results calculated with an evaluation point grid with 40 479 points only in the restricted region. Note that we again plot just a variation of the harmonic density distribution because we apply also in this section the gravitational potential only from degree 3 up to degree 360.
At first we have tried to reconstruct the harmonic density distribution from only a small number of data points (1 431) to get out the differences between each scale and each sequence with relatively short computing times, namely about five hours on an ordinary PC. Numerical tests (see [34]) turned out that the best recovery can be achieved by using the Abel-Poisson kernels which are presented in Fig. 3.

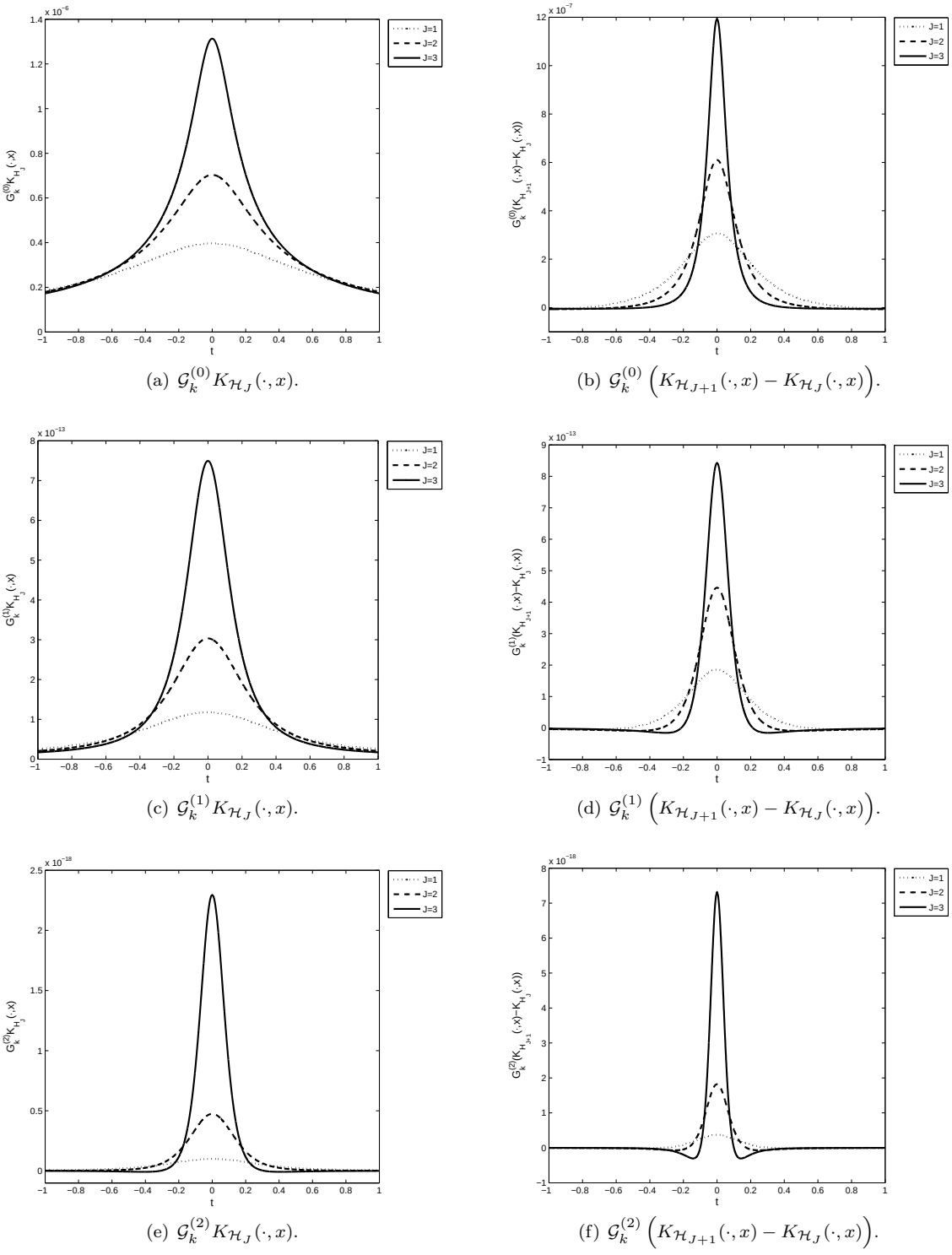

(a) $\mathcal{G}_k^{(0)} K_{\mathcal{H}_J}(\cdot, x)$.

(b) $\mathcal{G}_k^{(0)} \left(K_{\mathcal{H}_{J+1}}(\cdot, x) - K_{\mathcal{H}_J}(\cdot, x) \right)$.

(c) $\mathcal{G}_k^{(1)} K_{\mathcal{H}_J}(\cdot, x)$.

(d) $\mathcal{G}_k^{(1)} \left(K_{\mathcal{H}_{J+1}}(\cdot, x) - K_{\mathcal{H}_J}(\cdot, x) \right)$.

(e) $\mathcal{G}_k^{(2)} K_{\mathcal{H}_J}(\cdot, x)$.

(f) $\mathcal{G}_k^{(2)} \left(K_{\mathcal{H}_{J+1}}(\cdot, x) - K_{\mathcal{H}_J}(\cdot, x) \right)$.

Figure 3: Plot of the different Abel-Poisson kernels $\mathcal{G}_k^{(m)} K_{\mathcal{H}_J}(\cdot, x)$ (left column) and their differences $\mathcal{G}_k^{(m)} \left(K_{\mathcal{H}_{J+1}}(\cdot, x) - K_{\mathcal{H}_J}(\cdot, x) \right)$ (right column) for all $m \in \{0, 1, 2\}$ and all $J \in \{1, 2, 3\}$.

Therefore, we show in this paper only results computed with these kernels and have, firstly, analyzed the corresponding kernel matrices. In Fig. 4 we see an illustration of the different matrices concerning the different $m \in \{0, 1, 2\}$. For the computations we also distinguish the radii used for the several point grids. The calculations are done with the Abel-Poisson sequence at scale $J = 5$. If we consider these matrices, we can directly remark the symmetry, the different sizes of their entries and the bands which dominate the matrices. Since these matrices belong to the systems of linear equations one requires a detailed consideration concerning the condition and the rank of them. So, we explore especially the rank of the matrix for regularity.

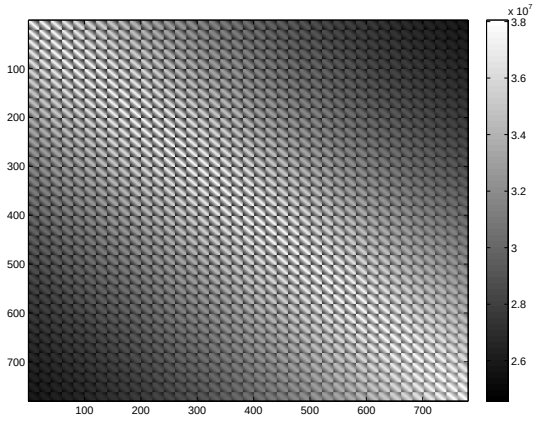

(a) $\mathcal{G}_i^{(0)}\mathcal{G}_k^{(0)}K_{\mathcal{H}_8}(\cdot,\cdot)$ computed almost at the Earth's surface.

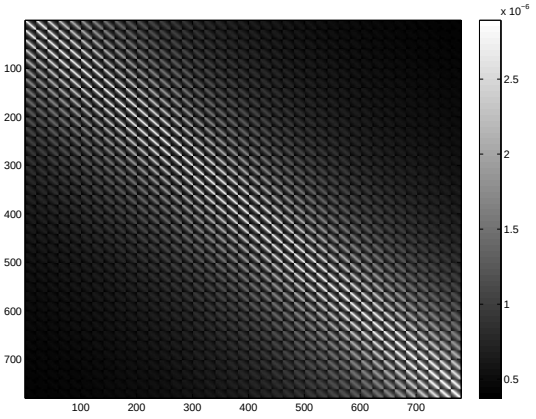

(b) $\mathcal{G}_i^{(1)}\mathcal{G}_k^{(1)}K_{\mathcal{H}_8}(\cdot,\cdot)$ computed in about 400 km altitude.

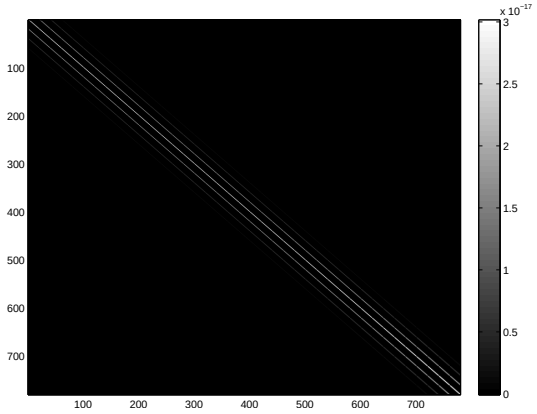

(c) $\mathcal{G}_i^{(2)}\mathcal{G}_k^{(2)}K_{\mathcal{H}_8}(\cdot,\cdot)$ computed in about 200 km altitude.

Figure 4: Plot of the different matrices $\mathcal{G}_i^{(m)}\mathcal{G}_k^{(m)}K_{\mathcal{H}_8}(\cdot,\cdot)$ of South America computed for an 780 point grid each generated with the different radii.

In our case, we find out that the property of the full rank is dependent on the scale, on the number of the points of their point grids and on the degree $\tilde{n} \in \mathbb{N}_0$ of the sum which we have to truncate for the realization. The Table 1 shows us the connections between these three variables. The values of this scheme represent such smallest $\tilde{n}$, which suffices for a regular matrix. For all calculations we apply the Abel-Poisson sequence and we choose $m = 0$, i.e. we compute the matrix only for the gravitational potential and not for its derivatives. Note that the entry "-" tells us, that we never attain a regular matrix regardless of which $\tilde{n}$ we apply.
Additionally to this table we can remark that for larger $\tilde{n}$ the condition number becomes smaller. But although we have regular matrices they are not well-conditioned.

number of data points	scale 3	scale 4	scale 5	scale 6	scale 7	scale 8
1 176	121	109	105	105	104	104
1 431	-	121	118	117	116	116
1 652	-	136	131	130	129	128
1 953	-	149	144	142	141	140
2 312	-	167	158	156	155	154
2 555	-	182	171	168	166	166
2 964	-	203	186	182	180	179
3 320	-	231	198	194	194	191
3 784	-	-	214	208	206	205
4 140	-	-	231	221	218	217
4 606	-	-	245	237	234	232
5 100	-	-	259	249	246	244
5 564	-	-	277	265	261	259
6 048	-	-	291	277	273	271
6 669	-	-	310	293	288	286
7 018	-	-	326	306	300	298

Table 1: Values of the degree $\tilde{n} \in \mathbb{N}_0$, from which the corresponding kernel-matrix has a full rank, that is for all $n \geq \tilde{n}$, $n \in \mathbb{N}_0$, the matrix was observed to be regular.

In total we observe that a relatively high, but numerically acceptable degree of truncation can yield well-conditioned, band-dominated matrices for a stable determination of the spline coefficients $a_1, \ldots, a_N$.

Now, we come to the results concerning the reconstruction of the harmonic density distribution. As we can see in Fig. 5(a) the number of data points is too small. Here, we can recognize each point itself because the kernel localizes already at scale $J = 4$ too intensively such that it makes no sense to consider results calculated at higher scales. Thus, we choose a data point grid, where the difference between two adjoint points is smaller (see thereto Fig. 5(b)).

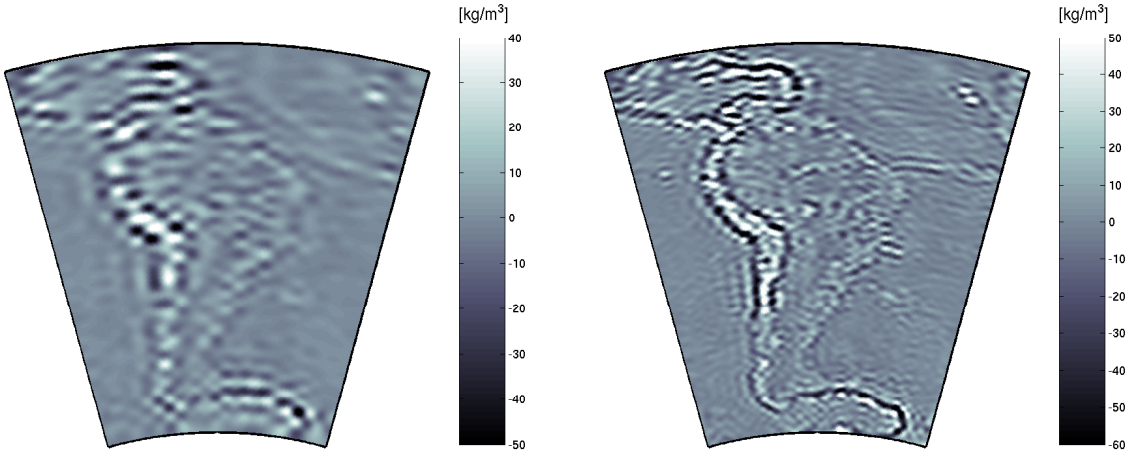

(a) Computed from 1 431 data points at scale $J = 4$, $\left(v_{\min} \approx -97\,\frac{\text{kg}}{\text{m}^3},\ v_{\max} \approx 67\,\frac{\text{kg}}{\text{m}^3}\right)$.

(b) Computed from 4 606 data points at scale $J = 4$, $\left(v_{\min} \approx -204\,\frac{\text{kg}}{\text{m}^3},\ v_{\max} \approx 235\,\frac{\text{kg}}{\text{m}^3}\right)$.

Figure 5: Variation of the harmonic density distribution calculated with the Abel-Poisson kernels.

However, for getting even better results, we use for the next plots (see Fig. 6) a point grid with 10 366 data points. By an input with such many data points we really obtain good results for the

harmonic density distribution and, now, it makes sense to calculate at higher scales, too, which can be seen in Fig. 6(b). Finally, for reasons of these good results, we can say that this spline interpolation method is a good approach for reconstructing the harmonic density distribution, mainly for detecting local details. For example, the Galapagos islands which are located in the west of South America show the good approximation via this spline interpolation method as we can clearly see them in these figures.

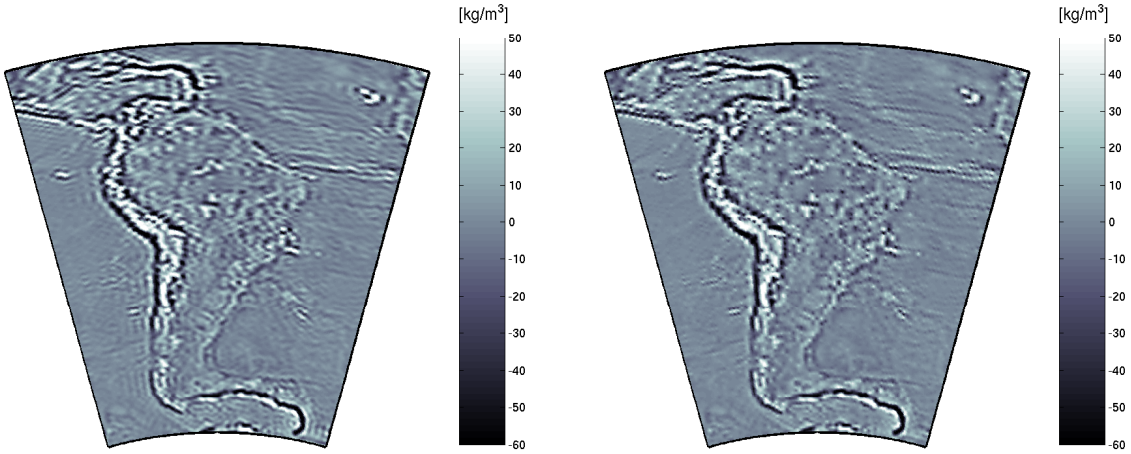

(a) $J = 4$, $\left(v_{\min} \approx -425\,\frac{\mathrm{kg}}{\mathrm{m}^3},\ v_{\max} \approx 260\,\frac{\mathrm{kg}}{\mathrm{m}^3}\right)$. (b) $J = 8$, $\left(v_{\min} \approx -333\,\frac{\mathrm{kg}}{\mathrm{m}^3},\ v_{\max} \approx 301\,\frac{\mathrm{kg}}{\mathrm{m}^3}\right)$.

Figure 6: Variation of the harmonic density distribution computed from 10 366 data points with the Abel-Poisson kernels.

Next, for comparison to well-known interpolation methods by the principle of a multiresolution analysis (see thereto, e.g., [24]), we demonstrate our results analogously. This means that we also illustrate the detail information which arises from the difference of the results of two consecutive scales. Thus, by increasing the scale and adding, simultanously, more data points the resolution becomes better and better which is clearly shown in Fig. 7. In this figure we see in the left column the spline S_J at different scales, $J \in \{6, 7, 8\}$, and in the right column the differences $S_{J+1} - S_J$ for $J \in \{6, 7\}$ representing detail information. Therefore, from the sum of the two reconstructions in each row it follows the left image of the proximate row. At the same time, we add also more and more data points and finally get for each higher scale a better resolution. In conclusion, the last image presents a quite good reconstruction of the harmonic density distribution calculated from the gravitational potential almost on the Earth's surface.

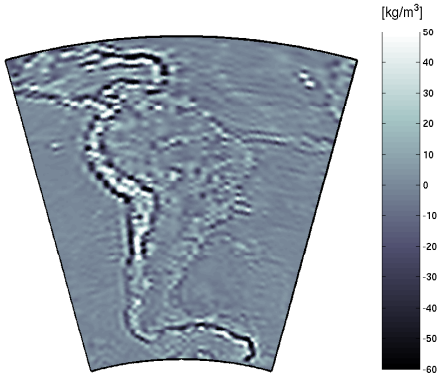

(a) S_6 computed from 4 606 points, $\left(v_{\min} \approx -201 \frac{\text{kg}}{\text{m}^3},\ v_{\max} \approx 268 \frac{\text{kg}}{\text{m}^3}\right)$.

+

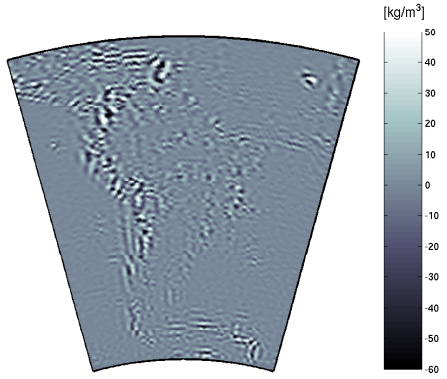

(b) $S_7 - S_6$, $\left(v_{\min} \approx -161 \frac{\text{kg}}{\text{m}^3},\ v_{\max} \approx 198 \frac{\text{kg}}{\text{m}^3}\right)$.

=

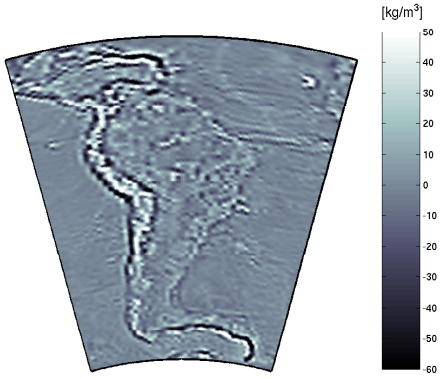

(c) S_7 computed from 7 018 points, $\left(v_{\min} \approx -249 \frac{\text{kg}}{\text{m}^3},\ v_{\max} \approx 268 \frac{\text{kg}}{\text{m}^3}\right)$.

+

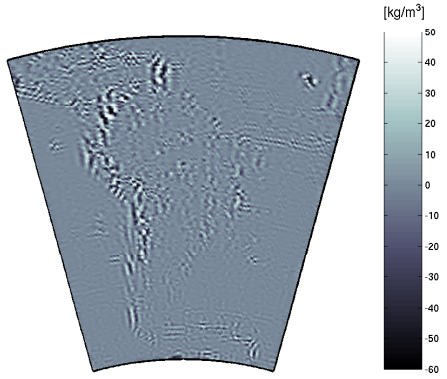

(d) $S_8 - S_7$, $\left(v_{\min} \approx -190 \frac{\text{kg}}{\text{m}^3},\ v_{\max} \approx 208 \frac{\text{kg}}{\text{m}^3}\right)$.

=

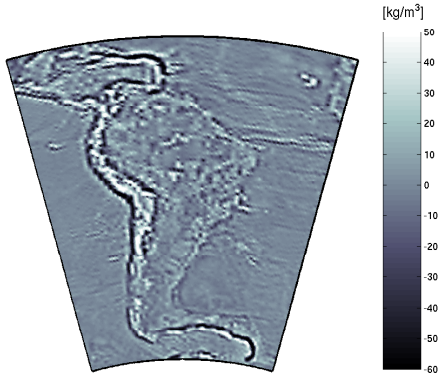

(e) S_8 computed from 10 366 points, $\left(v_{\min} \approx -333 \frac{\text{kg}}{\text{m}^3},\ v_{\max} \approx 301 \frac{\text{kg}}{\text{m}^3}\right)$.

Figure 7: Plot like a multiresolution for a variation of the harmonic density distribution, that is the plot of S_J in the left column and the plot of $S_{J+1} - S_J$ in the right column computed with the Abel-Poisson kernels for $J \in \{6, 7, 8\}$.

4.4 Combination of Several Data Sets

In the last two sections we have analyzed the reconstruction of the Earth's interior from gravitational data but, acually, we want to solve the gravimetry problem not only via the gravitational potential but also in combination with its first and second radial derivative. Thus, our aim is to reconstruct the Earth's harmonic density distribution which is computed from a data set given by the first radial derivative in 400 km altitude, a second data set given by the second radial derivative in 200 km altitude and, additionally, from a third data set which is given by the gravitational potential almost at the Earth's surface.
The different radii are chosen for reasons of the different satellite orbits. Data for the first radial derivative of the gravitational potential are given by CHAMP and GRACE which generate a data set in about 400 km altitude, and the second radial derivative is a part of SGG which generates a data set in approximately 200 km. Consequently, in this section, we show the first images of the harmonic density distribution calculated by combining several data sets. For the calculation of such a combination we get a matrix in which we can differ three parts on the diagonal. This matrix gives us a system of linear equations which has to be solved.
Fig. 8 presents the result of such a combination of three data sets with following properties:

1. 1 431 data points of the first radial derivative in 400 km altitude,
2. 2 555 data points of the second radial derivative in 200 km altitude,
3. 4 140 data points of the zeroth derivative almost on the Earth's surface.

On the left hand side, we see the original solution where we can clearly observe some boundary effects. To remove those implications of such calculations we add 5% to the values of the diagonal of the part concerning to the second radial derivative and 10% to the values of the diagonal of the part concerning to the first radial derivative. But although we can solve the problem of the boundary effects by such an appropriate regularization, we achieve a solution where several details are vanished because this method smoothes our original result. This is the tribute for the exponential ill-posedness of the downward continuation from satellite height.

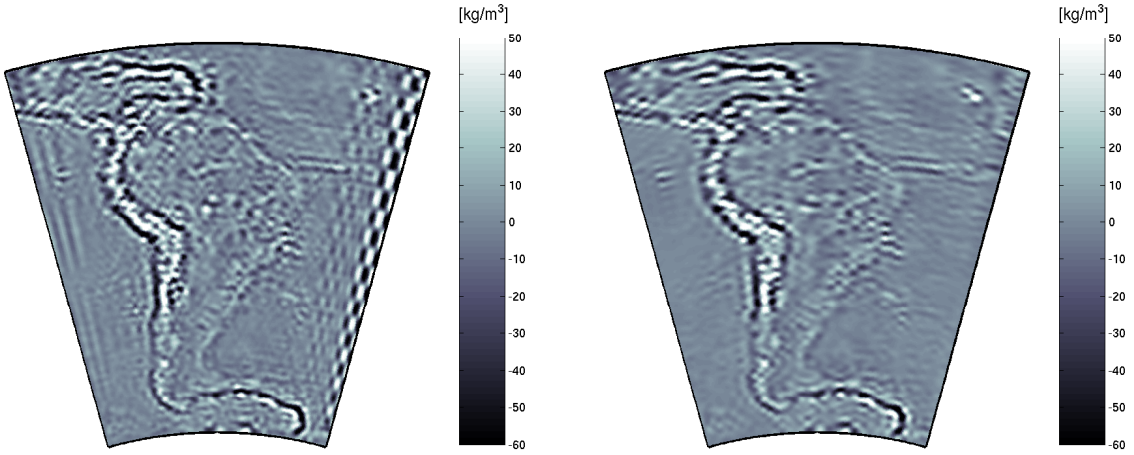

(a) Non-regularized solution, $\left(v_{\min} \approx -230\,\frac{\mathrm{kg}}{\mathrm{m}^3},\ v_{\max} \approx 196\,\frac{\mathrm{kg}}{\mathrm{m}^3}\right)$.

(b) Appropriate regularization with 5% and 10%, $\left(v_{\min} \approx -194\,\frac{\mathrm{kg}}{\mathrm{m}^3},\ v_{\max} \approx 172\,\frac{\mathrm{kg}}{\mathrm{m}^3}\right)$.

Figure 8: Combination of the data provided by the cases 1.-3. and computed with the Abel-Poisson kernel at scale $J = 5$

At last, we want to show that, by the harmonic spline interpolation method, we can "zoom" in an interesting area in order to achieve more details in this region. Therefore, we combine two different data sets. Firstly, we apply data points computed globally from the second radial

derivative of the gravitational potential which are located in 200 km altitude and, secondly, we use data points computed locally from the gravitational potential itself which are located almost on the Earth's surface. For the first data set we use for the calculation 6 320 data points distributed over the whole Earth and the second data set consists of 2 964 data points distributed only over the interesting region. For this region we have, therefore, as a start the few data which belong to the data set calculated for the whole Earth and in addition to those data we have the information which belong to the data set computed only for South America. This result is illustrated in Fig. 9. Again we have to choose a factor for regularizing because without such a perturbance in the matrix we do not achieve reasonable results due to the ill-posedness. This time we add 5% to the diagonal of the matrix which belongs to the data for the whole Earth. Then, we can clearly see more details of the harmonic density distribution in the region of South America, i.e. in the interesting area, whereas the rest represents the harmonic density distribution with less information. Hence, the method is indeed appropriate for mixing different data sets in order to achieve locally adapted resolutions of the results.

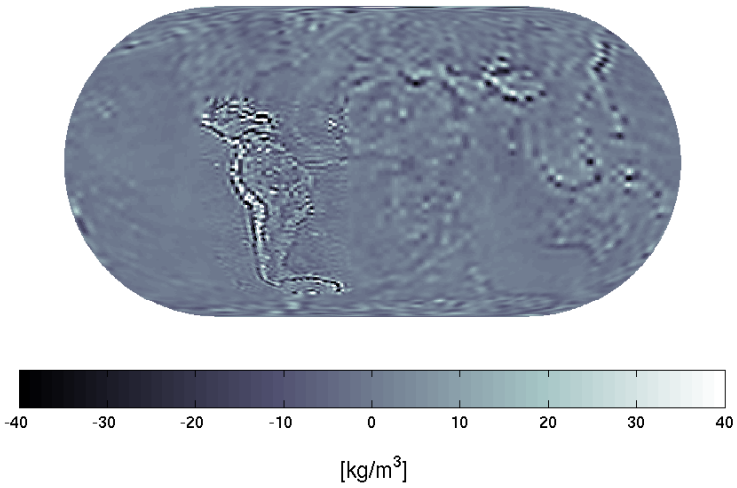

Figure 9: Appropriate regularization of a variation of the harmonic density distribution as a combination of 6 320 data points computed globally from the second radial derivative of the gravitational potential in about 200 km altitude and of, additionally, 2 964 data points computed locally from the gravitational potential itself almost at the Earth's surface. For both data sets we apply the Abel-Poisson kernel at scale $J = 5$, $\left(v_{\min} \approx -190\,\frac{\mathrm{kg}}{\mathrm{m}^3},\ v_{\max} \approx 131\,\frac{\mathrm{kg}}{\mathrm{m}^3}\right)$.

5 Conclusion

The numerical results presented in the last three sections illustrate the approximation properties of the harmonic spline interpolation method. More precisely, we discussed the application of this method to an exponentially ill-posed problem in geophysics and physical geodesy. With it, we are able to determine an approximation of the harmonic density distribution of the Earth by using gravitational data, i.e. we applied a method for solving the classical gravimetry problem.

For the numerical realization we have a closer look at the data which we use for the right hand side of the systems of linear equations. In reality, we obtain the data for the first radial derivative of the gravitational potential and also those for the second radial derivative at satellite

orbits. Therefore, we have to determine the Earth's mass density distribution out of gravitational information given outside the Earth. In particular, the gradient of the potential is part of SST generated on a point grid in about 400 km altitude and the Hessian of the potential is part of SGG generated on a point grid in about 200 km altitude. Additionally, there exist gravitational data obtained at the Earth's surface which we also want to apply for our solution.

Therefore, concerning the data the explained spline interpolation method can be well adapted to the real data situation. For our numerical realizations we indeed represented, for simplifications, the orbits and the Earth's surface by spheres with different radii, but for such an interpolation method the data need not be located any more on a sphere which is often simply assumed as an approximation to the satellite orbits. Another advantage is that we are able to combine different types of data, more precisely, to combine different derivatives of the gravitational potential. Such combinations of different data sets are shown in Fig. 8 and Fig. 9.
Furthermore, the larger the scale is chosen the smaller the hat-width of the basis functions becomes. Hence, in dependance on the different scales we have to choose a sufficiently dense data grid. Here, we meet problems caused by the memory capacity of our computers such that the number of the used data points is limited. We also discovered that for the bandlimited cases, such as the Shannon sequences and those generated by a cubic polynomial, we do not achieve such good approximations than for the Abel-Poisson kernels, especially for small scales. But for the Abel-Poisson kernels we achieve really good reconstructions of the harmonic density distribution of the Earth which we see in Fig 2(b). In addition, the resolution of the achieved solution can locally be varied by increasing the data points in the corresponding region. So, we selected the region of South America to solve, in the first instance, locally the gravimetry problem. We find out, that the harmonic spline interpolation method is a better method for exploring locally a region than for global calculations. After restricting to a small part of the whole Earth's surface we realize several details, like for example the Galapagos Islands.
At last, (see Fig. 9) we combine the global reconstruction from the satellite data and the local reconstruction from the data obtained at the Earth's surface and achieve a "zooming-in" image. This is also an interesting result based on the advantages of this spline interpolation method since, now, we have two differently dense point grids combined in one figure and correspondingly locally adapted resolutions of the result which is not achievable by polynomial approach.

6 Acknowledgments

The authors gratefully acknowledge the financial support by the German Research Foundation (DFG), project MI 655/2-1, and also by the German Federal Ministry of Education and Research (BMBF), project TIVAGAM.

References

[1] D.D. Ang, R. Gorenflo, and L.K. Vy. A Uniqueness Theorem for a Nonlinear Integral Equation of Gravimetry. Freie Universität Berlin, Fachbereich Mathematik, Serie A: Mathematik, Preprint No. A-29/92.

[2] L. Ballani, J. Engels, and E.W. Grafarend. Global Base Functions for the Mass Density in the Interior of a Massive Body (Earth). *Manuscripta Geodaetica*, 18:99–114, 1993.

[3] L. Ballani and D. Stromeyer. *The Inverse Gravimetric Problem: A Hilbert Space Approach.* Proceedings of the International Symposium 'Figure of the Earth, the Moon, and other Planets', P. Holota (ed.), Prague, 1982.

[4] L. Ballani and D. Stromeyer. On the Structure of Uniqueness in Linear Inverse Source Problems. In A. Vogel, A.K.M. Sarwar, R. Gorenflo, and O.I. Kounchev, editors, *Theory and Practice of Geophysical Data Inversion, Proceedings of the 8th International Mathematical*

Geophysics Seminar on Model Optimization in Exploration Geophysics, Vieweg Verlag, Braunschweig, Wiesbaden, 1990.

[5] L. Ballani, D. Stromeyer, and F. Barthelmes. Decomposition Principles for Linear Source Problems. In G. Anger, R. Gorenflo, H. Jochmann, H. Moritz, and W. Webers, editors, *Inverse Problems: Principles and Applications in Geophysics, Technology, and Medicine*. Mathematical Research, 74, Akademie-Verlag, Berlin, 1993.

[6] R. Barzaghi and F. Sansò. Remarks on the Inverse Gravimetric Problem. *Anno XIV - Bollettino di geodesia e scienze affini*, pages 203–216, 1986.

[7] C.W. Clenshaw. A Note on the Summation of Chebyshev Series. *Mathematical Tables and Other Aids to Computation*, 9:118–120, 1955.

[8] P. Deuflhard. On Algorithms for the Summation of Certain Special Functions. *Computing*, 17:37–48, 1975.

[9] J. Engels, E.W. Grafarend, and P. Sorcik. The Gravitational Field of Topographic-Isostatic Mases and the Hypothesis of Mass Condensation - Part I and II. *Schriftenreihe der Institute des Fachbereichs Vermessungswesen*. Universität Stuttgart, Report Nr. 1995.1.

[10] M.J. Fengler, D. Michel, and V. Michel. Harmonic Spline-Wavelets on the 3-dimensional Ball and their Application to the Reconstruction of the Earth's Density Distribution from Gravitational Data at Arbitrarily Shaped Satellite Orbits. *Zeitschrift für Angewandte Mathematik und Mechanik*, 86:131–146, 2006.

[11] W. Freeden and V. Michel. *Multiscale Potential Theory (with Application to the Geosciences)*. Birkhäuser, Boston, 2004.

[12] J. Goguel. *1st edition, La Gravimétrie*. Presses Universitaires de France, Paris, 1963.

[13] E. Groten. Some Remarks on Downward Continuation of Gravity. In Wilbur T. Kattner, editor, *Advances in Dynamic Gravimetry, Proceedings of the Symposium on Dynamic Gravimetry, March 16-17*, Fort Worth, Texas; Instrument Society of America, Pittsburgh, 1970.

[14] L.L. Helms. *Introduction to Potential Theory*. Wiley-Interscience, New York, 1969.

[15] K. Jung. Schwerkraftverfahren in der Angewandten Geophysik. *Geophysikalische Monographien*, 2, 1961. Akademische Verlagsgesellschaft Geest & Portig K.-G., Leipzig.

[16] S. Krappmann. *Zero-Potential Densities in Geodesy and Geophysics*. PhD thesis, Graz, 1996.

[17] B.J. Last and K. Kubik. Compact Gravity Inversion. *Geophysics*, 48:713–721, 1983.

[18] F.G. Lemoine, S.C. Kenyon, J.K. Factor, R.G.Trimmer, N.K. Pavlis, D.S. Chinn, C.M. Cox, S.M. Klosko, S.B. Luthcke, M.H. Torrence, Y.M. Wang, R.G. Williamson, E.C. Pavlis, R.H. Rapp, and T.R. Olson. *The Development of the Joint NASA GSFC and NIMA Geopotential Model EGM96*. NASA/TP-1998-206861. NASA Goddard Space Flight Center, Greenbelt, Maryland, USA, 1998.

[19] E. Lewi. *Modelling and Inversion of High Precision Gravity Data*. PhD thesis, Deutsche Geodätische Kommission bei der Bayerischen Akademie der Wissenschaften, München, 1997.

[20] V. Michel. A Wavelet Based Method for the Gravimetry Problem. In W. Freeden, editor, *Progress in Geodetic Science, Proceedings of the Geodetic Week 1998*. 283-298, Shaker Verlag, 1998.

[21] V. Michel. *A Multiscale Method for the Gravimetry Problem - Theoretical and Numerical Aspects of Harmonic and Anharmonic Modelling*. PhD Thesis, Geomathematics Group, Department of Mathematics, University of Kaiserslautern, Shaker Verlag, Aachen, 1999.

[22] V. Michel. *A Multiscale Approximation for Operator Equations in Separable Hilbert Spaces - Case Study: Reconstruction and Description of the Earth's Interior*. Habilitation Thesis, Geomathematics Group, Department of Mathematics, University of Kaiserslautern, Shaker Verlag, Aachen, 2002.

[23] V. Michel. Scale Continuous, Scale Discretized and Scale Discrete Harmonic Wavelets for the Outer and the Inner Space of a Sphere and Their application to an Inverse Problem in Geomathematics. *Applied and Computational Harmonic Analysis (ACHA)*, 12:77–99, 2002.

[24] V. Michel. Regularized Wavelet-based Multiresolution Recovery of the Harmonic Mass Density Distribution from Data of the Earth's Gravitational Field at Satellite Height. *Inverse Problems*, 21:997–1025, 2004.

[25] H. Moritz. *The Figure of the Earth: Theoretical Geodesy and the Earth's Interior*. Herbert Wichmann Verlag GmbH, Karlsruhe, 1990.

[26] L.L. Nettleton. Determination of Density for Reduction of Gravity Observations. *Geophysics*, 4:176–183, 1939.

[27] L.L. Nettleton. Geophysical Prospecting for Oil. 1940. McGraw-Hill, New York.

[28] F. Sansò, R. Barzaghi, and C.C. Tscherning. Choice of Norm for the Density Distribution of the Earth. *Geophys. J. R. atr. Soc.*, 87:123–141, 1986.

[29] F.J Simons, R.D. van der Hilst, and M.T. Zuber. Spatiospectral localization of isostatic coherence anisotropy in Australia and its relation to seismic anisotropy: Implications for lithospheric deformation. *Journal of Geophysical Research*, 108, 2003.

[30] F.J Simons, M.T. Zuber, and J. Korenaga. Isostatic response of the Australian lithosphere: Estimation of effective elastic thickness and anisotropy using multitaper spectral analysis. *Journal of Geophysical Research*, 105, 2000.

[31] M. Thalhammer, Y. Ricard, R. Rummel, and K.H. Ilk. Application of Spaceborne Gravimetry to Research on the Interior of the Earth. 1996. ESA Study - CIGAR 4, Final Report.

[32] C.C. Tscherning and H. Sünkel. A method for the construction of spheroidal mass distributions consistent with the harmonic part of the Earth's gravity potential. *Manuscripta Geodaetica*, 6:131–156, 1981.

[33] W. Walter. *Einführung in die Potentialtheorie*. BI, Mannheim, 1971.

[34] K. Wolf. Numerical Aspects of Harmonic Spline Wavelets for the Satellite Gravimetry Problem. Diploma Thesis, Geomathematics Group, Department of Mathematics, University of Kaiserslautern, 2006.

Folgende Berichte sind erschienen:

2003

Nr. 1 S. Pereverzev, E. Schock.
On the adaptive selection of the parameter in regularization of ill-posed problems

Nr. 2 W. Freeden, M. Schreiner.
Multiresolution Analysis by Spherical Up Functions

Nr. 3 F. Bauer, W. Freeden, M. Schreiner.
A Tree Algorithm for Isotropic Finite Elements on the Sphere

Nr. 4 W. Freeden, V. Michel (eds.)
Multiscale Modeling of CHAMP-Data

Nr. 5 C. Mayer
Wavelet Modelling of the Spherical Inverse Source Problem with Application to Geomagnetism

2004

Nr. 6 M.J. Fengler, W. Freeden, M. Gutting
Darstellung des Gravitationsfeldes und seiner Funktionale mit Multiskalentechniken

Nr. 7 T. Maier
Wavelet-Mie-Representations for Soleniodal Vector Fields with Applications to Ionospheric Geomagnetic Data

Nr. 8 V. Michel
Regularized Multiresolution Recovery of the Mass Density Distribution From Satellite Data of the Earth's Gravitational Field

Nr. 9 W. Freeden, V. Michel
Wavelet Deformation Analysis for Spherical Bodies

Nr. 10 M. Gutting, D. Michel (eds.)
Contributions of the Geomathematics Group, TU Kaiserlautern, to the 2nd International GOCE User Workshop at ESA-ESRIN Frascati, Italy

Nr. 11 M.J. Fengler, W. Freeden
A Nonlinear Galerkin Scheme Involving Vector and Tensor Spherical Harmonics for Solving the Incompressible Navier-Stokes Equation on the Sphere

Nr. 12 W. Freeden, M. Schreiner
Spaceborne Gravitational Field Determination by Means of Locally Supported Wavelets

Nr. 13 F. Bauer, S. Pereverzev
Regularization without Preliminary Knowledge of Smoothness and Error Behavior

Nr. 14 W. Freeden, C. Mayer
Multiscale Solution for the Molodensky Problem on Regular Telluroidal Surfaces

Nr. 15 W. Freeden, K. Hesse
Spline modelling of geostrophic flow: theoretical and algorithmic aspects

2005

Nr. 16 M.J. Fengler, D. Michel, V. Michel
Harmonic Spline-Wavelets on the 3-dimensional Ball and their Application to the Reconstruction of the Earth's Density Distribution from Gravitational Data at Arbitrarily Shape Satellite Orbits

Nr. 17 F. Bauer
Split Operators for Oblique Boundary Value Problems

Nr. 18 W. Freeden, M. Schreiner
Local Multiscale Modelling of Geoidal Undulations from Deflections of the Vertical

Nr. 19 W. Freeden, D. Michel, V. Michel
Local Multiscale Approximations of Geostrophic Flow: Theoretical Background and Aspects of Scientific Computing

Nr. 20 M.J. Fengler, W. Freeden, M. Gutting
The Spherical Bernstein Wavelet

Nr. 21 M.J. Fengler, W. Freeden,
A. Kohlhaas, V. Michel, T. Peters
Wavelet Modelling of Regional and Temporal Variations of the Earth's Gravitational Potential Observed by GRACE

Nr. 22 W. Freeden, C. Mayer
A Wavelet Approach to Time-Harmonic Maxwell's Equations

Nr. 23 M.J. Fengler, D. Michel, V. Michel
Contributions of the Geomathematics Group to the GAMM 76th Annual Meeting

Nr. 24 F. Bauer
Easy Differentiation and Integration of Homogeneous Harmonic Polynomials

Nr. 25 T. Raskop, M. Grothaus
On the Oblique Boundary Problem with a Stochastic Inhomogeneity

2006

Nr. 26 P. Kammann, V. Michel
Time-Dependent Cauchy-Navier Splines and their Application to Seismic Wave Front Propagation

Nr. 27 W. Freeden, M. Schreiner
Biorthogonal Locally Supported Wavelets on the Sphere Based on Zonal Kernel Functions

Nr. 28 V. Michel, K. Wolf
Numerical Aspects of a Spline-Based Multiresolution Recovery of the Harmonic Mass Density out of Gravity Functionals

TECHNISCHE UNIVERSITÄT
KAISERSLAUTERN

Informationen:

Prof. Dr. W. Freeden
Prof. Dr. E. Schock
Fachbereich Mathematik
Technische Universität Kaiserslautern
Postfach 3049
D-67653 Kaiserslautern
E-Mail: freeden@mathematik.uni-kl.de
schock@mathematik.uni-kl.de